CRYSTAL GROWTH & DESIGN

pubs.acs.org/crystal

Article

Access to Enantiomeric Organic Compounds with Potential for Synthesis via Racemic Conglomerates: Inositol Derivatives as a Case in Point

Nivedita T. Patil, Madhuri T. Patil, Nitai Sarkar, Rajesh G. Gonnade,* and Mysore S. Shashidhar*

Cite This: *Cryst. Growth Des.* 2021, 21, 3786−3797

Read Online

ACCESS | Metrics & More | Article Recommendations | Supporting Information

ABSTRACT: The crystal structure database was used to identify inositol derivatives that could be crystallizing as racemic conglomerates. Among the six racemic inositol derivatives identified, racemic 4-*O*-tosyl-6-*O*-benzyl-*myo*-inositol-1,3,5-orthoformate (A) was found to be a true conglomerate and was resolved on the multigram scale by the preferential crystallization technique. This resolution procedure does not require the use of any enantiomeric resolving agent. The resolved enantiomers of A are useful for the synthesis of natural and unnatural enantiomeric derivatives of inositol, since they carry orthogonal hydroxy protecting groups. Racemic 4-*O*-methanesulfonyl-*myo*-inositol-1,3,5-orthoformate (B) on crystallization from common organic solvents generally yielded racemic twin crystals, while in the presence of structural analogs as additives, they yielded true racemic crystals. A comparison of the crystal structures of the true racemate, twinned crystal and crystal of one of the enantiomers of B, revealed the reasons for the formation of polymorphic (twin) crystals. Such instances are relatively rarely encountered but nevertheless shed light on our understanding of polymorphism and twinning of crystals.

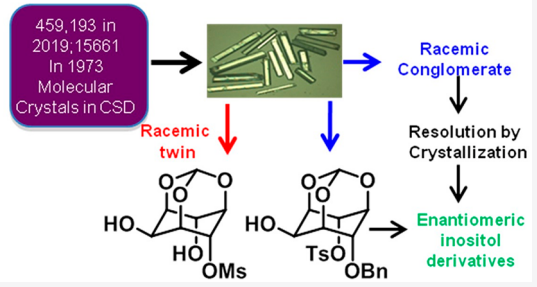

INTRODUCTION

A perusal of the chemistry literature published in the last few decades reveals the extent of effort devoted to the synthesis and study of chiral molecular entities. Synthesis of enantiomerically pure organic compounds and resolution of racemates have gained unprecedented significance due to different properties of enantiomers and racemates, *e.g.*, the therapeutic efficacy of drugs.[1−4] Enantiomeric organic compounds can be extracted routinely from natural sources, although with wide variation in inputs in terms of cost, effort, and time. Due to the high enantiomeric purity of organic compounds isolable from natural sources, many of them form the starting materials for the synthesis of natural and unnatural chiral molecular entities.[5−9] Most laboratory methods of preparation of enantiomeric compounds involve the use of enantiomeric molecular entities such as catalysts (including enzymes) for asymmetric synthesis, chiral auxiliaries, resolving agents, or chiral stationary phases for the separation of enantiomers (in a racemate).[3,10−14] Almost all of these methods to obtain enantiomers depend on the solution-state chemistry. Enantiomers present in a racemate can also be separated by preferential enrichment of enantiomers[15] and by preferential crystallization of conglomerates.[16] Interestingly, the separation of enantiomers by such a simple crystallization process does not require the use of any external enantiopure entity and, hence, require relatively less effort to scale up (as compared to chemical methods of separation of enantiomers).

Generally, a racemic compound can crystallize as racemate, kryptoracemates (chiral racemates), conglomerate, solid solution, or scalemic (anomalous racemates, Figure S1, SI).[17−20] Racemate crystals (90−95% of the cases) belong to non-Sohncke space groups and contain an equal amount of both enantiomers in regular order in the crystal lattice. In kryptoracemate (0.8% cases), the asymmetric unit of the crystal structure is comprised of both enantiomers ($Z' = 2$ or even numbers) in equal numbers and the racemate crystallizes in Sohncke space groups.[21] Conversely, in conglomerates (5−10% cases), both enantiomers are spontaneously resolved and crystallize separately. Each crystal is enantiopure, belonging to a Sohncke space group, and the crystal structures of the two enantiomers have a mirror symmetry relationship. The "racemic twin" crystals are a different kind of conglomerate crystals (lamellar conglomerate)[22] wherein each crystal comprises separate domains (lamellae) of both enantiomers and each domain contains only one of the two enantiomers and the crystal belongs to a Sohncke space group. In solid solutions (1−2% cases),[18,19,21] although both enantiomers are

Received: February 2, 2021
Revised: June 3, 2021
Published: June 15, 2021

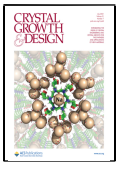

https://doi.org/10.1021/acs.cgd.1c00126
Cryst. Growth Des. 2021, 21, 3786−3797

present in equal quantity, they are randomly distributed (irregular arrangement of enantiomers) in the crystal lattice, with no long-range periodicity. Solid solution can crystallize in non-Sohncke or Sohncke space groups. In the scalemic racemates[19,21] (anomalous racemate, 37 structures are reported in Cambridge Structural Database — CSD), the stoichiometric ratio of the two enantiomers is other than 1*R*:1*S*. The scalemic racemates are rarer than kryptoracemates and crystallize in Sohncke space groups. The rare occurrence of scalemics could be due to fewer crystallization studies from nonracemic mixtures. Among these solid forms of racemates, several conglomerates and few twin crystals have been resolved to their enantiomers by crystallization techniques. Although preferential crystallization of racemic conglomerates has the potential to provide enantiomers rapidly, this method of resolution has limitations in that not all racemates are solids and only a small percentage (~5−10%) of solid racemates exist as conglomerates under ambient conditions.[16,17,21]

There has been an upsurge in interest in the synthesis of cyclitols, their phosphorylated derivatives and the associated lipids in the recent past because of the biological roles played by phosphoinositols in living cells.[23−28] The intense biological studies aimed at understanding the *myo*-inositol cycle and its implication in several diseases led to a demand for enantiopure synthetic inositol derivatives.[29,30] Although inositol derivatives have been prepared using a variety of starting materials, naturally occurring *myo*-inositol is the most preferred starting material because of its abundance and well-developed chemistry.[30−32] However, the limitation of this approach is that since *myo*-inositol has the *meso*-configuration, preparation of its enantiomeric derivatives and analogs necessitates the resolution of racemates or the use of enantiopure catalysts and, more often than not, tedious and labor intensive separation and purification procedures. Since a large number of isomeric products are generated during the derivatization of *myo*-inositol,[33] the majority of the known methods for the preparation of enantiopure inositol derivatives have resorted to the use of partially protected *myo*-inositol derivatives (which have fewer hydroxy groups, such as *myo*-inositol orthoesters) to generate enantiomeric derivatives.[29−32,34] We realized that a large number of inositol derivatives exist as crystalline solids and hundreds of crystal structures were reported in the CSD. Hence, identifying and resolving inositol derivatives that could function as versatile synthetic intermediates by preferential crystallization of conglomerates appeared practical. This article reports our efforts in realizing the resolution of a racemic *myo*-inositol derivative (conglomerate) into its enantiomers by preferential crystallization.[16] This approach is more or less an absolute asymmetric synthetic approach,[35] since no enantiopure molecular entity is used to obtain enantiomeric end products. During this work, we also encountered a *myo*-inositol derivative that exhibited polymorphism depending on the crystallization conditions wherein one of the crystal forms was a racemic twin and the other polymorph was a true racemate. The significance of the study of the crystal structure of twinned racemates is the fact that the intricacies of the twinning phenomena could shed light on energetics and mechanisms of nucleation and crystal formation.

RESULTS AND DISCUSSION

Since a racemic conglomerate is a physical mixture of enantiopure crystals, it crystallizes in a Sohncke space group, and the powder X-ray diffraction profiles of the racemic mixture and pure enantiopure crystals are identical.[16] A survey of the CSD 2020 (version November 2019) for the crystal structure of inositol derivatives revealed that among 416 derivatives, 130 crystallized in Sohncke space groups. Of these 130 entries, 54 were diastereomeric derivatives of *myo*-inositol, and among the 76 remaining *myo*-inositol derivatives, 41 were enantiopure compounds, 28 were *meso*-derivatives, and 7 were racemates (Scheme 1).[36−41] A perusal of our own (unpublished) crystal structure database revealed that the racemic tosylate **Rac6**[42] crystallized in the orthorhombic Sohncke space group $P2_12_12_1$.

Scheme 1. Racemic Inositol Derivatives Which Are Known to Crystallize in Sohncke Space Groups (Rac1, Rac2, Rac5—$P2_1$; Rac3, Rac4, Rac6, Rac7—$P2_12_12_1$)[a]

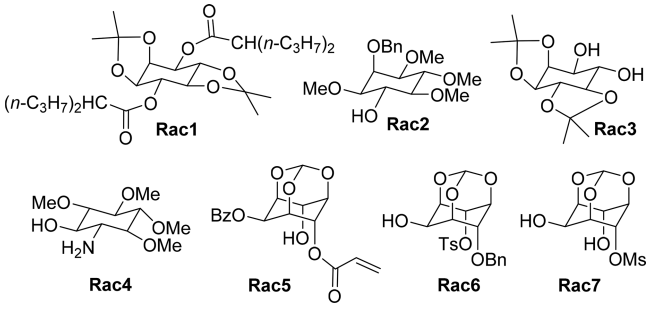

[a]The molecular structure of one of the enantiomers is shown for brevity.

Among the racemic inositol derivatives which crystallized in the Sohncke space group, **Rac1**−**Rac4** seemed unsuitable as versatile synthetic intermediates, while the orthoformate derivative **Rac5** revealed molecular crystal polymorphism. One of the polymorphs was a true racemate (crystallized in triclinic $P\bar{1}$ centrosymmetric space group), while the other crystallized as a rarely encountered kryptoracemate[43] in the monoclinic $P2_1$ Sohncke space group, with two molecules of the enantiomeric pair in the asymmetric unit.[38] Hence, we did not attempt to resolve **Rac1**−**Rac5**. The racemic sulfonates **Rac6** and **Rac7** were amenable to synthetic transformations due to orthogonally protected hydroxy groups (benzyl ether, tosylate/mesylate, and orthoformate), and we had earlier used sulfonate esters of inositol for the synthesis of several naturally occurring inositol derivatives.[44−47] Accordingly, a detailed investigation of the crystallization behavior of **Rac6** and **Rac7** and their resolution by preferential crystallization of enantiomers was pursued.

The racemic tosylate **Rac6** was prepared as shown in Scheme 2, starting from commercially available **8** in an overall yield of 30% over five steps. The racemic tosylate **Rac6** can also be obtained in three steps from **8**,[42] but the synthetic sequence shown in Scheme 2 is more suited for preparation on a gram scale. Crystals of the tosylate **Rac6** exhibited all the characteristics of a racemic conglomerate: (a) the melting point of a single crystal (182−184 °C) was higher than that of a random mixture of crystals (152−154 °C); (b) the simulated powder X-ray diffraction (PXRD) pattern from a single crystal X-ray diffraction data and experimental PXRD pattern of a random crystalline mixture of **Rac6** were identical (Figure S2, SI); (c) chiral HPLC analysis of a mixture of crystals showed the presence of both enantiomers in the ratio 1:1 (Figure S3a, SI), while that of single crystal showed the presence of a single

https://doi.org/10.1021/acs.cgd.1c00126
Cryst. Growth Des. 2021, 21, 3786−3797

Scheme 2. Preparation of the Tosylate Rac6[a]

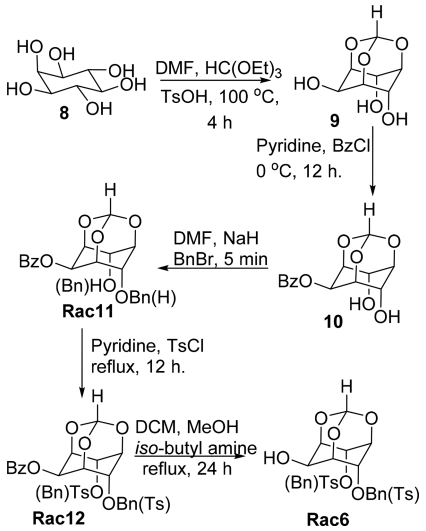

[a]Compounds **Rac6**, **Rac11**, and **Rac12** are racemic, while **8**, **9**, and **10** have the *meso*-configuration; Bz = C_6H_5CO-; Bn = $C_6H_5CH_2-$; Ts = *p*-$CH_3C_6H_4SO_2-$.

enantiomer (Figure S3b, SI).[48] Crystals weighing at least 1 mg were initially obtained from a solution of **Rac6** in ethyl acetate. We could use only one of these crystals for seeding the first crystallization experiment (during resolution), since we had no clue about the absolute configuration of the constituent molecules of different individual crystals. However, the fact that **Rac6** crystallized as a conglomerate guaranteed that all the constituent molecules within a single crystal had the same configuration (Figure S4, SI). By an iterative crystallization procedure, we could achieve resolution of **Rac6** on a gram scale (Scheme 3, Figure S5, SI).[48]

We determined the visual melting range of various mixtures of **D6** and **L6** and realized that this data could be used as a guideline to follow the resolution of **Rac6** by crystallization (Tables S3–S5, SI). The melting range of the enantiomerically enriched crystals approached 179–181 °C toward the end of resolution by repeated crystallization. The optimum duration for crystallization 1 was 25 min (see the Experimental Section for details) to obtain enantiomeric ratios of 80:20 or better. Allowing crystallization 1 to proceed for more than 25 min resulted in reduced enantiomeric excess (Tables S4–S5, SI). Hence, this melting range data allowed the tracking of enantiomerically enriched samples (by measuring the melting range) obtained during the preferential crystallization of enantiomers from **Rac6** and circumvented the need for HPLC analysis after each crystallization step, during the process of resolution. However, the enantiomeric purity of both resolved enantiomers was confirmed by chiral HPLC analysis. The absolute configuration of the resolved enantiomeric tosylates was established by single-crystal X-ray diffraction analysis (anomalous dispersion effects, Flack parameter was 0.02(6) and 0.04 (3), respectively, for **D6** and **L6** crystals), which showed that **D6** was (+)-1D-4-*O*-tosyl-6-*O*-benzyl-*myo*-inositol-1,3,5-orthoformate and **L6** was (−)-1L-4-*O*-tosyl-6-*O*-benzyl-*myo*-inositol-1,3,5-orthoformate. This agrees with the fact that the known (+)-1D-2,4-di-*O*-benzyl-*myo*-inositol (**D14**, Scheme 3)[49] was obtained[48] from **L6**. The benzyl ether **D14** is a precursor for the preparation of 1L-*myo*-inositol-1,3,4,5-tetrakisphosphate.[13,49] Hence, in principle, this constitutes a formal synthesis of the latter enantiomeric tetrakisphosphate, without the aid of any external optically active molecular entity.

The advantage of the present method of using **D6** and **L6** for the preparation of enantiopure compounds is that neither any enantiopure reagent nor the intervention of diastereomeric derivatives is necessary to arrive at enantiopure synthons or end products. All the previously reported approaches for the preparation of enantiopure inositol derivatives involved enantiopure reagents or (more often than not, chromatographic) separation of diastereomeric derivatives (and conversion of the separated diastereomers back to enantiomers). Since all the functional groups (an ether, a tosylate, a hydroxy group, and the orthoformate) in **D6** and **L6** are orthogonal, these chiral derivatives have high synthetic potential as versatile intermediates. "Absolute asymmetric synthesis" is a term used to imply the generation of optical activity—without the use of any chiral agent or environment.[50] Synthesis of enantiopure end products involving the resolution of a conglomerate using a homochiral crystal as a seed for the preferential crystallization of enantiomers is close to this approach, since the formation of a conglomerate is an intrinsic property of a particular racemate and does not require the use of any external enantiopure agent or environment. The formation of enantio-enriched molecules via reactions in chiral crystals comprising of achiral molecules is another example of "Absolute asymmetric synthesis".[51] Incidentally, the processes of generation of enantiomers without the aid of enantiopure agents are also of immense relevance to understanding the occurrence and evolution of homochirality in nature.

Crystal Structure of D6 and L6. Single-crystal structure determination revealed that both enantiomers crystallized in the frequently encountered orthorhombic Sohncke space group $P2_12_12_1$ containing a single molecule in the asymmetric unit (Figure S6, SI). The crystal structure analysis showed adamantane-like geometry for the *myo*-inositol orthoformate moiety, whereas the pincer-like benzyl and tosyl groups were in

Scheme 3. Resolution of Rac6 by Preferential Crystallization of Enantiomers from a Solution in Ethyl Acetate–Acetonitrile Mixture[48a]

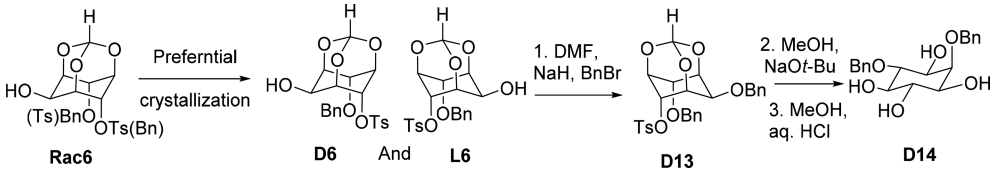

[a]The purity of the resolved enantiomers was >99%, as revealed by chiral HPLC analysis (Figure S5, SI). The known **D14** could be obtained from **L6**.

https://doi.org/10.1021/acs.cgd.1c00126
Cryst. Growth Des. 2021, 21, 3786–3797

extended and folded conformation, respectively. The closely associated molecules generated a helical architecture along the crystallographic 2_1-screw axis (*b*-axis) through O—H···O═S (O2—H2A···O8) hydrogen bonding interactions (Figure 1a).

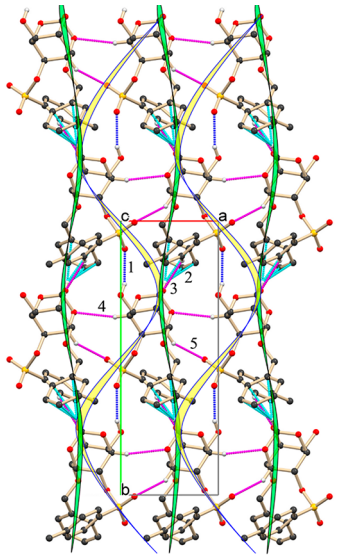

(a) 1. O2-H2A…O8 2. C7-H7…Cg5 3. C20-H20...O3 4. C3-H3…O5 5. C5-H5...O7

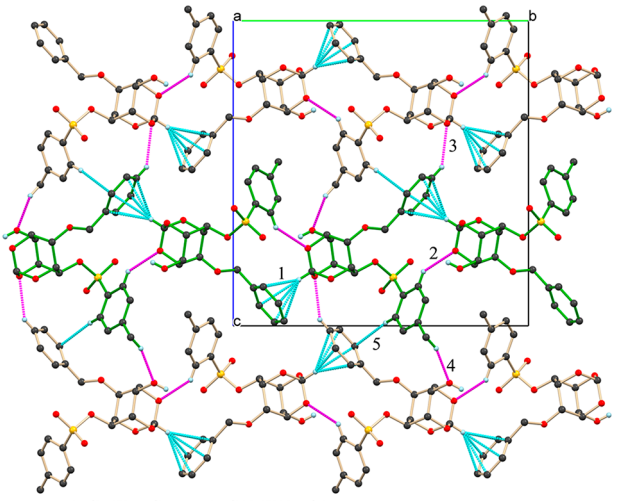

(b) 1. C7-H7...Cg5 2. C16-H16...O1 3. C12-H12...O3 4. C21-H21B...O2 5. C20-H19...Cg5

Figure 1. Molecular packing viewed down the (a) *c*-axis and (b) *a*-axis showing the linking of the adjacent C—H···π helices. Intermolecular interactions are indicated by blue (O—H···O), magenta (C—H···O), and cyan (C—H···π) colors. The yellow and green strips in (a) show helices linked via O—H···O and C—H···π interactions, respectively.

Another helical assembly connected the 2_1-screw-related molecules along the *b*-axis by highly directional C—H···π (C7—H7···Cg5 engaging orthoformate H atom and π cloud of the phenyl ring of benzyl group) interactions supplemented by a C—H···O (C16—H16···O1) interactions. Both these helices are intermingled and run in a parallel fashion along the *b*-axis. Adjacent C—H···π linked helices are unit-translated through O—H···O and C—H···O (C3—H3···O5 and C5—H5···O7) interactions along the shorter *a*-axis to reveal a compact packing on the *ab* plane (Figure 1b). The view of molecular arrangement on the *bc* plane revealed the stitching of C—H···π linked helices through C—H···O (C12—H12···O3, C16—H16···O1, C21—H21B···O2) interactions engaging phenyl rings of the benzoyl and tosyl groups (Figure 1).

The approximate energy for the intermolecular potential, which is the sum of Coulombic, polarization, dispersion, and repulsion terms (as defined in the PIXEL method[52,53] and integrated into the program Mercury[54]) was calculated using UNI force field computations. The estimation of potential energy values for the intermolecular interactions revealed that the molecules were strongly associated (−64.8 kJ/mol) along the shortest *a*-axis (Figure 1b). The packing of molecules along *b*- and *c*-axes were relatively weak (Figure 1b), as indicated by potential energy values for C—H···π (−29.7 kJ/mol) and O—H···O═S (−26.9 kJ/mol) interactions. Along the *c*-axis wherein the adjacent helices are connected through tosyl moiety via C—H···O and moderate C—H···π interactions, the intermolecular potential energy value was −44.6 kJ/mol. This suggests that the association of the molecules along the *a*-axis could have been swift (compared to those along *b*- and *c*-axes) because of the relatively stronger binding affinity making it the fastest growing face. This is corroborated by the needle-shaped crystals of **D6** and **L6**. The Bravis, Friedel, Donnay, and Haker (BFDH) morphology study[55,56] also substantiated the rod shape of the crystal, revealing that either [101] (red) or [110] (green) is the fastest-growing face (Figure 2).

It has also been suggested that the growth rate of a plane is inversely proportional to the interplanar spacing, and the growth is faster along a direction having smaller distance spacing.[55,56] Although we cannot visualize the nucleation process, we can speculate that the association of the molecules along the shortest *a*-axis (Figure 1b) to form a one-dimensional chain could have been step-1 of the crystallization event. The subsequent growth of these 1D polymers along the *b*-axis (through O—H···O and strong C—H···π interactions) (Figure 1b) could have been step-2 and packing of the neighboring helices along the *c*-axis (through C—H···O contacts) could have been step-3 (Figure 1a). Hence, the strong interactions between the homochiral molecules, particularly along the *a*-axis, seem to have been responsible for spontaneous resolution and conglomerate formation.

Crystallization Behavior of the Mesylate Rac7. The racemic mesylate **Rac7** was prepared by the mesylation of the racemic dibenzoate **Rac15** with methanesulfonyl chloride followed by methanolysis of the two benzoates in the presence of an excess of triethylamine.[36] The enantiomeric mesylate **D7** was prepared by mesylation of the known[57] dicamphanate **D17** followed by aminolysis of the camphanates (Scheme 4).

Crystallization of **Rac7** from chloroform−methanol mixture (1:1, v:v) at ambient conditions by slow evaporation over 3 days gave crystals (**Form I**, mp. 147 °C). Crystallization of **Rac7** in the presence of additives ((*R*)-(−)-mandelic acid or *myo*-inositol-1,3,5 orthoformate, about 2% by weight) from a 1:1 mixture (v:v) of chloroform and methanol at ambient conditions by slow evaporation over 24 h gave crystals (**Form II**, mp. 139−141 °C) (Figure S7, SI). We used the additives during the crystallization of **Rac7** since we suspected that crystallization of pure samples of **Rac7** yielded twinned crystals, while crystallization in the presence of certain impurities yielded a true racemate. Generally, isostructural additives are used as seeds to crystallize polymorphs,[58,59] wherein the interactions between the additive and the solute molecules aid in the enrichment of the different crystalline

https://doi.org/10.1021/acs.cgd.1c00126
Cryst. Growth Des. 2021, 21, 3786−3797

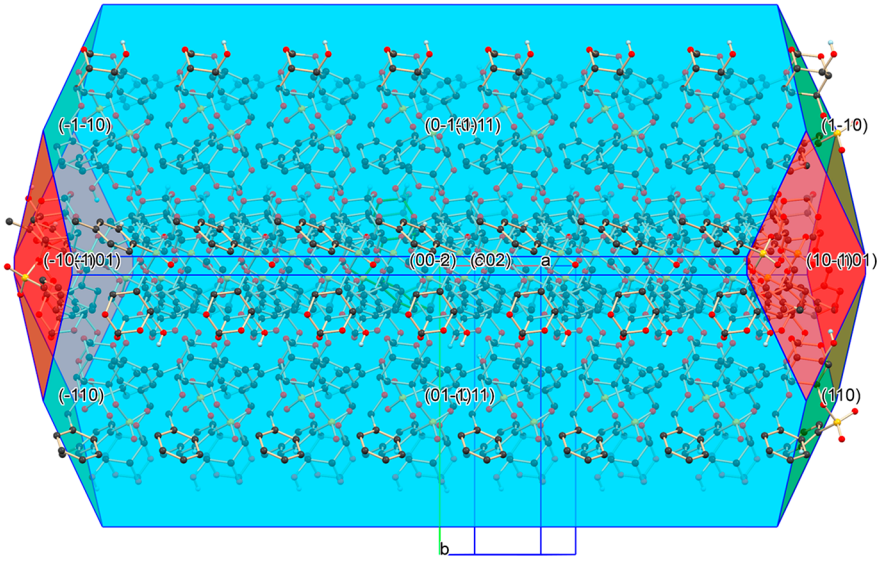

Figure 2. BFDH morphology calculations of **L6**.

Scheme 4. Synthesis of the Racemic and Enantiomeric Mesylates Rac7 and D7

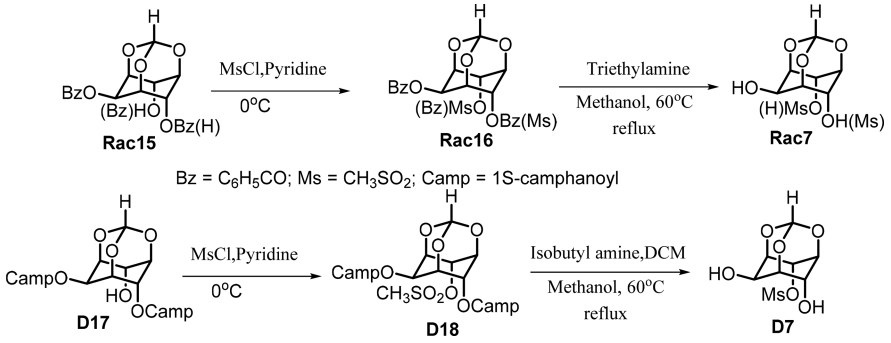

phases. In the present case, the additive *myo*-inositol-1,3,5 orthoformate offers some structural similarity with **Rac7**, but ((*R*)-(−)-mandelic acid does not. Hence, it is not easy to predict how the additive molecules provided nucleation sites for the generation of stable **Form II** crystals. However, we feel that the epitaxial interaction between nucleation promoting surface of additive and prenucleation aggregate of **Form I** crystals selectively inhibits **Form I** nucleation and promotes the growth of stable **Form II**. The enantiomer **D7** was crystallized from chloroform−methanol mixture (1:1, v/v, mp. 152−154 °C).

A bulk sample of crystalline mesylate **Rac7** had a melting point of 139−141 °C, while an isolated single crystal, crystallized from chloroform−methanol mixture of **Rac7**, had a higher melting point of 145−154 °C which suggested the possibility of **Rac7** being conglomerate crystals. DSC analysis of **Form I** and **Form II** crystals of **Rac7** and crystals of **D7** showed only the melting endotherm at 143 °C, 137 °C, and 153 °C, respectively (Figure S8, SI). This indicated the absence of phase transitions before the melting of crystals and that **Forms I** and **II** were not thermally interconvertible. The experimental PXRD patterns of **Form I** and **Form II** are different and showed a good match with their respective simulated PXRD pattern calculated from the single crystal X-ray diffraction data (Figure S9, SI). Furthermore, chiral HPLC analysis of individual single crystals of **Rac7** (**Form I**) showed that the ratio of enantiomers present in them varied from crystal to crystal, but none was a true racemate nor homochiral (Figure S10, SI). These results suggested that the crystals of the racemic mesylate **Rac7** (**Form I**) were not a true conglomerate.

Single-crystal X-ray diffraction analysis revealed that **Form I** crystals of **Rac7** and crystals of **D7** belonged to the orthorhombic $P2_12_12_1$ Sohncke space group, whereas **Form II** crystals of **Rac7** crystallized in the centrosymmetric monoclinic $C2/c$ space group, each containing one molecule in the asymmetric unit (Figure S11, SI). The unit cell parameters of **Form I** crystals of **Rac7** and crystals of **D7** were identical revealing isostructurality (see Experimental Section). However, their Flack parameter values differed (0.62(14) for **Form I** and −0.07(8) for **D7** crystals), indicating that the **Form I** crystals could be a racemic twin (having both enantiomers in single crystals). These results (along with DSC and HPLC analysis) confirmed the presence of different domains of the two enantiomers in **Form I** crystals of **Rac7**. A comparison of the scanning electron micrographs of **Form I**, **Form II** crystals of **Rac7**, and crystals of **D7** revealed epitaxial twinning in **Form I** crystals due to the stacking of the layers (Figures S12−S14, SI). **Form II** crystals of **Rac7** and crystals of **D7** contained no perforation and were evenly stacked, resulting in the formation of block or plate-shaped crystals. The crystal density values of **Form I**, **Form II**, and **D7** were 1.735, 1.741, and 1.722 g/cm^3, respectively, revealing that the molecules in racemic crystals (**Form II**) were closely packed as

https://doi.org/10.1021/acs.cgd.1c00126
Cryst. Growth Des. 2021, 21, 3786−3797

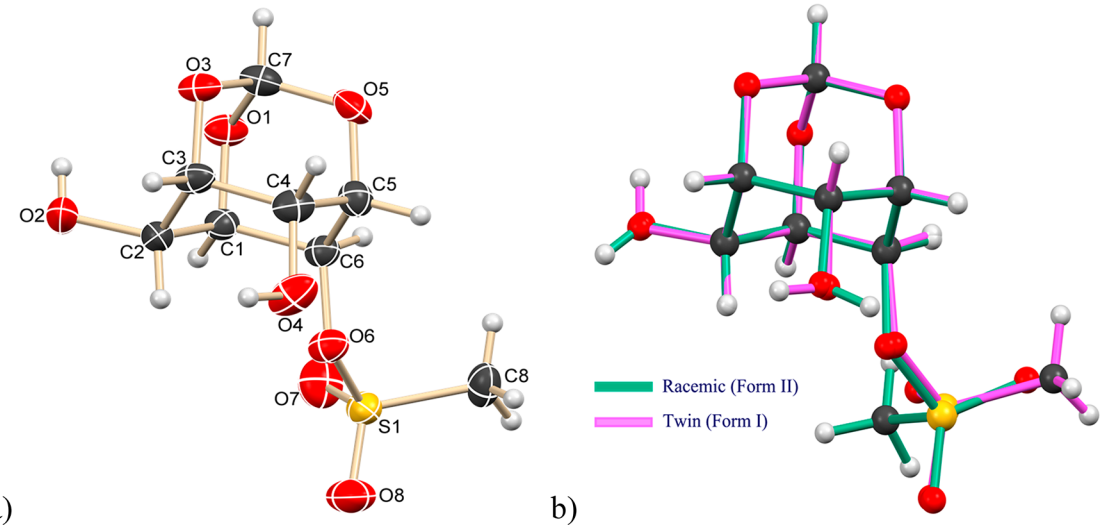

Figure 3. (a) ORTEP of **Rac7** (**Form I**) showing the numbering of atoms; (b) structural overlay of molecules in **Form I** (pink) and **Form II** (green) crystals of **Rac7**.

compared to twinned (**Form I**) and enantiopure (**D7**) crystals; the packing energy calculation also corroborates this. The estimation of packing energy for **Form I**, **Form II**, and **D7** crystals gave the values of −165.6, −177.4, and −164.1 kJ/mol, respectively, indicating that the **Form II** crystals are relatively more stable compared to **Form I** crystals. The results also validate the Wallach rule, which states that molecules in racemic crystals are packed more densely than their chiral counterparts.[60,61] These results clearly showed that **Rac7** did not crystallize as a true conglomerate.

The crystal structure analysis revealed identical conformation of molecules in **Form I** crystals of **Rac7** and crystals of **D7**, while the conformation of molecules in **Form II** crystals of **Rac7** was different (Figure 3 and Figure S15, SI). The structural overlay of the molecules in polymorphs **Forms I** and **II** of **Rac7** revealed the change in the orientation of the hydroxy and mesylate groups.

In both **Form I** and crystals of **D7**, the H atom of the 2-hydroxy group is pointed toward the orthoformate moiety (torsion angle, C1−C2−O2−H2A = −53.35°), whereas in the **Form II** crystals, it is pointing away from the orthoformate group (torsion angle, C1−C2−O2−H2A = 153.46°). Further, the H atom of the 4-hydroxy group also showed significant differences (114.67°) in conformation; in **Form I**, the torsion angle C3−C4−O4−H4A was −53.98°, whereas in **Form II**, it was 165.65°. Additionally, the mesylate group also displayed a considerable conformational difference (140.07°), the torsion angle C6−O6−S1−C8 was 72.32° and −67.75° for **Form I** and **Form II**, respectively. These conformational differences manifested in the dissimilar molecular arrangement leading to polymorphism in crystals of **Rac7**.

In **Form I** crystals, molecules assemble helically along the crystallographic 2_1-screw axis (*b*-axis) using conventional O—H···O hydrogen bonds (Figure 4a). The hydroxy group O4−H4A donates its H atom to the other hydroxy group oxygen, O2, to form O4−H4A···O2 hydrogen bonds. The helical association also brings the molecules related by unit-translation symmetry into close proximity to form O2−H2A···O4 hydrogen bonds and weak C8−H8A···O1 contacts. The neighboring helices along the *c*-axis are stitched through mesylate moieties using C8−H8B···O7, C8−H8C···O8, and C6−H6···O7 interactions; however, the association of the adjacent helices is relatively weak (Figure 4a). The molecular association along the *a*-axis also revealed a helical assembly formed along the *b*-axis through relatively weak interactions engaging mesylate moieties using C6−H6···O7, C8−H8B···O7, and C5−H5···O8 contacts. The unit-translated molecules along this helix are connected via the C7−H7···O2 hydrogen bond (Figure 4b). The neighboring helices along the longer *c*-axis are connected through O—H···O hydrogen bonds involving O4−H4A and O2 moieties supported by a C4−H4···O3 hydrogen bond to form 2D compact packing on the *ac*-plane.

Form II crystal structure revealed a helical assembly of molecules through C—H···O interactions (C7−H7···O7, C6−H6···O5, and C8−H8A···O5) across the crystallographic 2_1-screw axis (yellow or green, Figure 5a). The neighboring helices along the *a*-axis are stitched centrosymmetrically through conventional O2−H2A···O4 hydrogen bonds to generate the 2D layered assembly on the *ab*-plane (Figure 5a). A view of the molecular packing along the *c*-axis revealed the formation of one-dimensional molecular string (yellow or green) through conventional bifurcated O—H···O (O4−H4A···O2 and O4−H4A···O3) hydrogen bonds (blue) supplemented by C5−H5···O3 and C3−H3···O8 interactions (cyan). Successive molecules along the string have *c*-glide symmetry. The neighboring strings along the *a*-axis are centrosymmetrically stitched through O2−H2A···O4 (magenta) and C8−H8B···O8 (cyan) interactions to form a one-dimensional layered assembly parallel to the *c*-axis. The adjacent layers along the *a*-axis are connected through C7−H7···O7, C6−H6···O5, and C8−H8A···O5 contacts (cyan) to have a compact packing arrangement on the *ac* plane (Figure 5b).

As mentioned earlier, the racemic twin structure of **Form I** crystals was supported by SEM images, which revealed a lamellar domain structure, possibly consisting of alternate layers of two enantiomers leading to a non-racemic macroscopic composition. It has been assumed that the growth of the lamellar conglomerates occurs in phases from the solution containing an equal amount of both enantiomers.[22] First, homochiral microcrystals of both enantiomers nucleate

https://doi.org/10.1021/acs.cgd.1c00126
Cryst. Growth Des. 2021, 21, 3786−3797

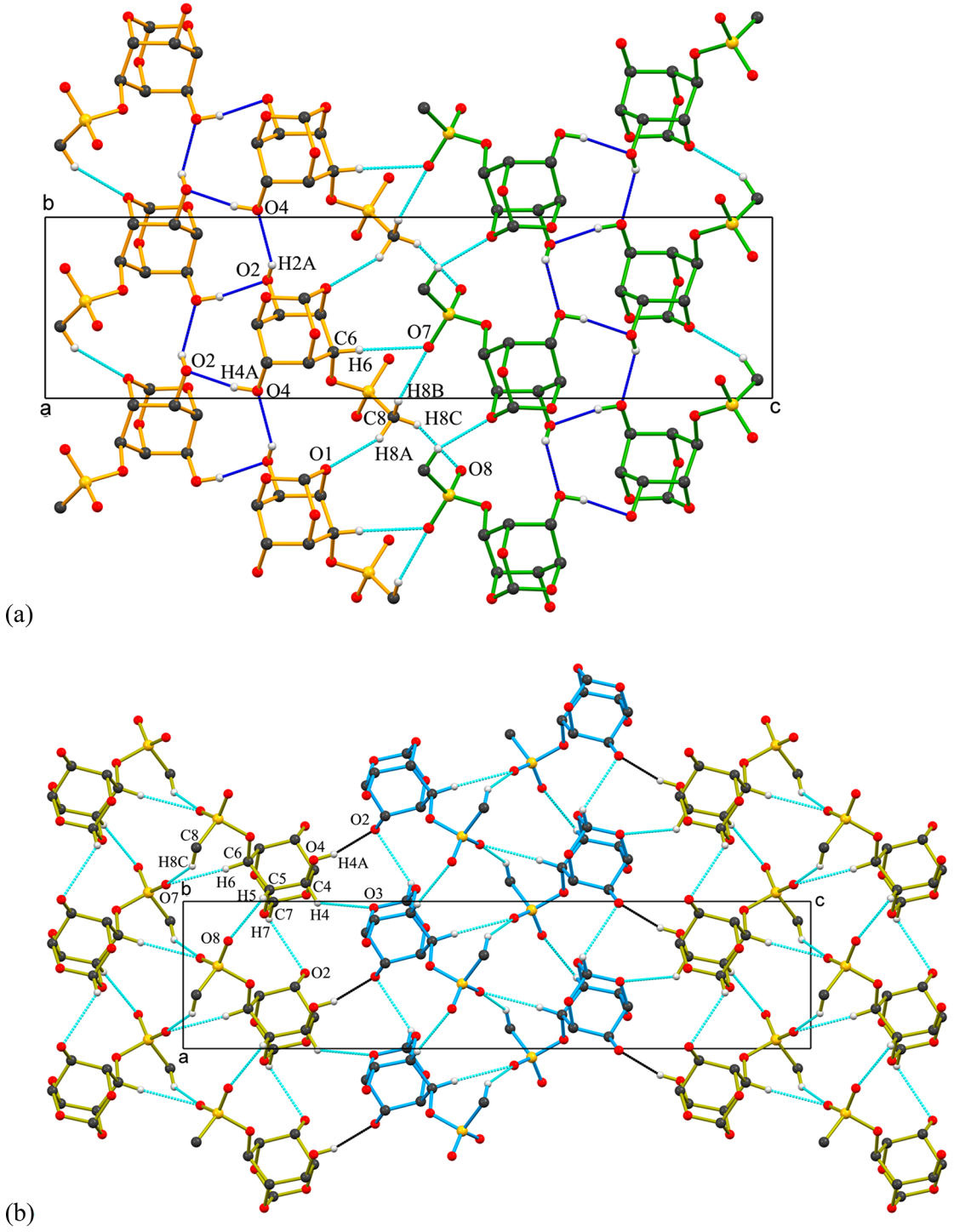

Figure 4. View of molecular packing in **Form I** crystals of **Rac7** showing the helical assemblies formed by O—H···O hydrogen bonds (a) and C—H···O interactions (b). The molecular arrangement in crystals of **D7** is the same as in **Form I** crystals. The different color used for the molecules is only for the identification of helices.

spontaneously to serve as crystallization initiators, the seed crystals. It is followed by the layering of both the Lemellae on one of the crystal faces of the seed crystals, alternately to yield the lamellar conglomerate crystals of varying thicknesses. Hence, the number of alternating lamellae of both enantiomers in the final crystal differ, thereby yielding the lamellar conglomerate crystals with an unequal proportion of both enantiomers. This could be the reason the chiral HPLC analysis of single crystals of **Form I** of **Rac7** showed variation in enantiomeric excess. This has also been supplemented by determining the Flack parameter (0.62(14)) of the single crystal using single-crystal X-ray diffraction.

The lamellar structure appeared along the slowest growing face of the crystal (transverse to the plate, along the longer *c*-axis), revealing a weak association between both enantiomers. Face indexing of the lamellar crystals (Figures S16–S18, SI) showed it to be the (001) face. In an attempt to gain better insight into the twin growth, we compared the energy values of

https://doi.org/10.1021/acs.cgd.1c00126
Cryst. Growth Des. 2021, 21, 3786–3797

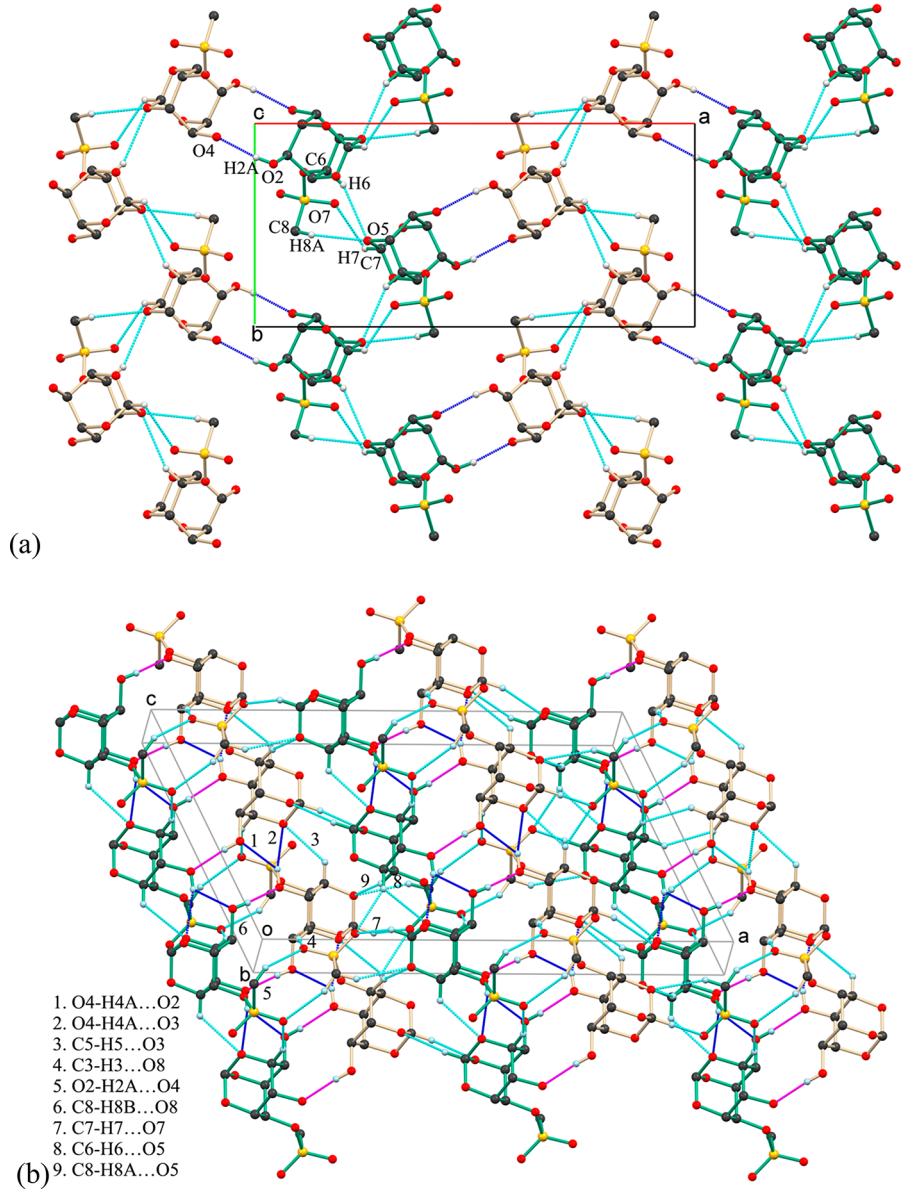

Figure 5. View of molecular packing in **Form II** crystal of **Rac7** (a) down *c*-axis; (b) down *b*-axis. The molecules are densely packed in (b) using O—H···O (blue and magenta) hydrogen bonds and several C—H···O (cyan) contacts.

intermolecular interaction potentials between neighboring molecules in dimorphs of **Rac7**. The energy values for the intermolecular potential were calculated using UNI force field computations.[52,53] The estimation of the intermolecular potential energies[54] for the strongest molecular pairs in **Forms I** and **II** revealed that the robust pairwise interaction between molecules in **Form II** crystals was a centrosymmetric O—H···O hydrogen bonding interaction (O2−H2A···O4, −52.0 kJ mol^{-1}), which is significantly stronger than any pairwise interaction in **Form I** crystals. A closer look at both enantiopure crystals of **D7** and racemic (**Form II**) crystal structures indicated that the centrosymmetric O—H···O hydrogen bonding interaction might have led to the formation of the junction between the two enantiomers and is possibly the crucial association in the early nucleation steps that lead to the twin boundary. According to Parsons,[62] the twinning is generally observed if the intermolecular interactions across the twin boundary are energetically competitive with that observed in single crystals.[22,62] The longer *c*-axis in **Form I** crystals could be due to the weak association of the molecules through C—H···O interactions involving mesylate moieties. The possible association of molecules of both enantiomers along the twin boundary in **Form I** crystals is depicted in Figure 6.

CONCLUSIONS

The existence of enantiomeric compounds was first realized due to the process of spontaneous resolution and conglomerate formation.[63−66] Separation of enantiomers from racemic conglomerates has been used for the preparation of active pharmaceutical ingredients,[67,68] and instances of resolution of conglomerates of certain organic compounds are reported in the literature, but the enantiomeric products obtained had very limited utility in organic synthesis.[69−71] However, this approach has been underutilized for the multistep organic synthesis of enantiomeric organic compounds (natural products and analogs, compounds of biological relevance or significance, etc.). As illustrated in the present work with inositol derivatives, identification of multifunctional organic

https://doi.org/10.1021/acs.cgd.1c00126
Cryst. Growth Des. 2021, 21, 3786−3797

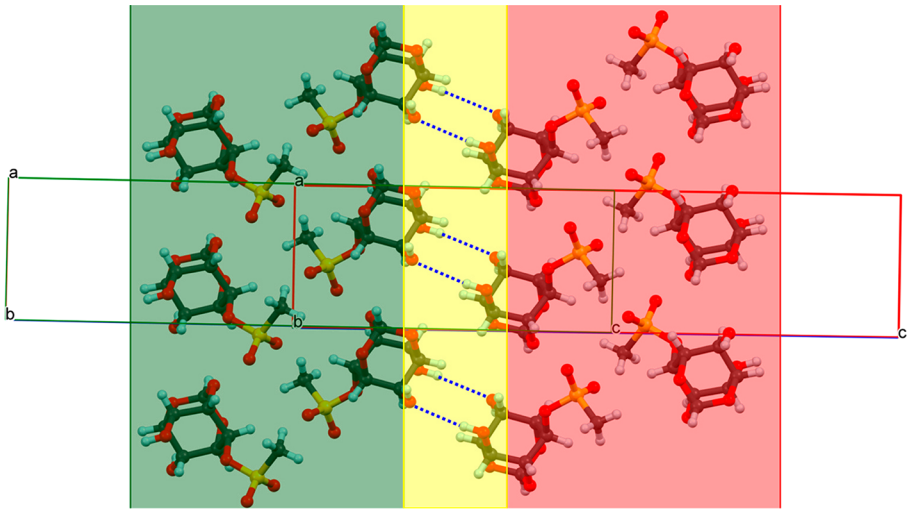

Figure 6. Depiction of the possible boundary between *S* (green) and *R* (red) enantiomorphs of **Rac7** in **Form I** crystals. The association is shown along the longest *c*-axis. The strong centrosymmetric pairs found in **Form II** are located in the yellow overlap region. Blue dashed lines indicate close O—H···O hydrogen bonds between the two enantiomers. The unit cells of both enantiomers of **Form I** were overlapped to reveal the possible junction in the lamellar twin crystals.

Table 1. Crystal Data Table

Crystal Data	D6	L6	Rac7, Form I	Rac7, Form II	D7
Crystal system	orthorhombic	orthorhombic	orthorhombic	monoclinic	orthorhombic
Formula	$C_{21}H_{22}O_8S$	$C_{21}H_{22}O_8S$	$C_8H_{12}O_8S$	$C_8H_{12}O_8S$	$C_8H_{12}O_8S$
Molecular weight	434.44	434.44	268.24	268.24	268.24
Crystal Size	0.51 × 0.28 × 0.18	0.43 × 0.22 × 0.15	0.35 × 0.32 × 0.25	0.45 × 0.32 × 0.21	0.45 × 0.32 × 0.21
Space group	$P2_12_12_1$	$P2_12_12_1$	$P2_12_12_1$	$C2/c$	$P2_12_12_1$
a (Å)	6.1403(2)	6.2115(17)	6.1053	21.469(12)	6.1039
b (Å)	17.4424(6)	17.488(5)	6.4741	8.978(6)	6.5048
c (Å)	18.0617(6)	18.342(5)	25.977	11.756(8)	26.0647
α (deg)	90	90	90	90	90
β (deg)	90	90	90	115.431(3)	90
γ (deg)	90	90	90	90	90
V (Å^3)	1934.44 (11)	1992.4 (9)	1026.8(2)	2046.5(2)	1034.89(3)
Z	4	4	4	8	4
D_{calc}, gcm^{-3}	1.492	1.448	1.735	1.741	1.722
μ, mm^{-1}	0.217	0.210	0.347	0.348	0.345
$F(000)$	912	912	560	1120	560
ab correct	multiscan	multiscan	multiscan	multiscan	multiscan
T_{min}/T_{max}	0.928/0.958	0.860/0.975	0.8881/0.9182	0.8589/0.9304	0.8466/0.8688
$2\theta_{max}$, deg	28.325, 100%	29.995, 100%	25°, 100%	25°, 100%	25°, 99.9%
Total refln.	28057	16881	6730	7873	7215
Unique refln.	4828	5786	1776	1809	1827
Obs. refln.	4658	5288	1730	2024	1782
h, k, l	h = −8, 8	h = −8, 6	h = −6, 7	h = −25, 25	h = −8, 7
	k = −23, 23	k = −24, 24	k = −7, 7	k = −10, 10	k = −7, 7
	l = −24, 24	l = −25, 25	l = −28, 30	l = −13, 13	l = −30, 26
R_{int}	0.0321	0.0456	0.0551	0.0490	0.0651
No. of parameters	273	273	157	157	157
$R1$ [$I > 2\sigma$]	0.0290	0.0377	0.0402	0.0308	0.0283
$wR2$ [$I > 2\sigma$]	0.0703	0.0953	0.1169	0.0806	0.0693
$R1$ [all data]	0.0302	0.0424	0.0425	0.0408	0.0289
$wR2$ [all data]	0.0709	0.0987	0.1235	0.0833	0.0696
Goodness of fit (S)	1.054	1.025	1.038	1.069	1.070
$\Delta\rho_{max}$ (e A^{-3}), $\Delta\rho_{max}$	0.305, −0.312	0.254, −0.348	0.321, −0.336	0.236, −0.416	0.221, −0.259
Flack Parameters	0.02(6)	0.04(3)	0.62(14)	-	−0.07(8)
CCDC No.	1875351	1875355	2055199	2055198	2055200

https://doi.org/10.1021/acs.cgd.1c00126
Cryst. Growth Des. 2021, 21, 3786−3797

compounds that crystallize as conglomerates, their resolution by preferential crystallization, and their development as chiral pool molecules is an approach worth investigating and/or pursuing. This approach seems practical due to the recent swelling of the crystal structure database. There have been attempts at using readily available *myo*-inositol as a starting material for the synthesis of natural products and their analogs.[34] As mentioned earlier, perhaps the main limitation for this was the nonavailability of enantiopure inositol derivatives in relatively large amounts; the method described herein circumvents this lacuna. The presence of an unequal proportion of the two enantiomers as in crystals **Form I** of **Rac7** is due to energetically competitive intermolecular interactions between the two enantiomers across the twin boundary. Although this twinning of crystals can be viewed as an obstacle to the resolution of racemates by crystallization, the crystal structure data helps understand the nonformation of true conglomerates.

EXPERIMENTAL SECTION

Resolution of the Tosylate Rac6. Seed crystals of the individual enantiomers **D6** and **L6** were available to us from previous work.[48] The two enantiomers were mixed in various proportions, and the melting range of the mixtures was determined. This data could be used to estimate the extent of enantiomeric enrichment or resolution achieved in individual crystallization experiments. Table 1 contains the crystallograpic data.

Three Gram Scale Resolution. Crystallization 1. The racemic tosylate **Rac6** (3 g) was suspended in a mixture of ethyl acetate (50 mL) and acetonitrile (10 mL) and stirred at 50−60 °C to obtain a clear solution. To this clear warm solution, crystals of the enantiomer **D6** (0.03 g) were added and stirred (at 450 rpm) for 25 min, while the solution was allowed to cool in the air. The precipitated **crystals A** were filtered (0.24−0.25 g); the range of melting point of enriched samples was between 165 and 175 °C; the ratio of enantiomers was in the range ∼80:20−90:10 (as revealed by the melting range, Tables S3−S5, SI). The mother liquor was evaporated to dryness under reduced pressure to obtain a **solid A** (2.5−2.6 g).

Crystallization 2. The **solid A** obtained above was mixed with **Rac6** (0.24−0.25 g, to make up to 3 g) and subjected to fractional crystallization as above (using the seed crystals of **L6**) when the enriched **crystals B** were obtained (0.24−0.25 g); the range of melting point of enriched samples were between 165 and 175 °C; the ratio of enantiomers were ∼20:80−10:90 (as revealed by the melting range, Tables S3−S5, SI).

These crystallization experiments 1 and 2 were repeated nine times each (total of about 7 g of **Rac6** was used in 18 crystallization experiments) to accumulate **crystals A** and **crystals B** (2.45 g each) enriched with the two enantiomers **D6** and **L6**.

Crystallization 3. **Crystals A** (2.45 g) were dissolved in ethyl acetate (45−60 mL), and the solution was allowed to stand open to the atmosphere for about 12 h. The crystals of **D6** obtained (1.96 g) were filtered and stored under reduced pressure to remove traces of solvents; mp. 178−182 °C; $^{25}[\alpha]_D$ = +1.98°. The enantiomer **L6** (1.95 g) was obtained from **crystals B** as above; mp. 178−182 °C; $^{25}[\alpha]_D$ = −1.72°. The enantiomeric purity of the resolved enantiomers (>99%) was confirmed by chiral HPLC analysis (Figure S5, SI).

ASSOCIATED CONTENT

Supporting Information

The Supporting Information is available free of charge at https://pubs.acs.org/doi/10.1021/acs.cgd.1c00126.

Experimental details for the preparation of **Rac6**, **D7**, **D13**, **D14**, and **D18** along with relevant compound characterization data; HPLC profiles for **Rac6**, **D6**, **L6**, and **Rac7**, and crystal structure data for **D6**, **L6**, **Rac7** (**Form I**), **Rac7** (**Form II**), **D7**, and **D18** along with interaction table; PXRD data for **Rac6** and **Rac7**; DSC data for **Rac7** (**Form I**), **Rac7** (**Form II**), and **D7**; SEM images for **Rac7** (**Form I**), **Rac7** (**Form II**), and **D7** (PDF)

Accession Codes

CCDC 1875351, 1875355, and 2055198−2055201 contain the supplementary crystallographic data for this paper. These data can be obtained free of charge via www.ccdc.cam.ac.uk/data_request/cif, or by emailing data_request@ccdc.cam.ac.uk, or by contacting The Cambridge Crystallographic Data Centre, 12 Union Road, Cambridge CB2 1EZ, UK; fax: +44 1223 336033.

AUTHOR INFORMATION

Corresponding Authors

Rajesh G. Gonnade − *Physical and Materials Chemistry Division, National Chemical Laboratory, Pune 411008, India; Academy of Scientific and Innovative Research, Ghaziabad, Uttar Pradesh 201002, India;* orcid.org/0000-0002-2841-0197; Phone: +91-20-25902225; Email: rg.gonnade@ncl.res.in

Mysore S. Shashidhar − *Division of Organic Chemistry, National Chemical Laboratory, Pune 411008, India; Academy of Scientific and Innovative Research, Ghaziabad, Uttar Pradesh 201002, India;* orcid.org/0000-0002-8477-1149; Email: ms.shashidhar@ncl.res.in

Authors

Nivedita T. Patil − *Division of Organic Chemistry, National Chemical Laboratory, Pune 411008, India; Academy of Scientific and Innovative Research, Ghaziabad, Uttar Pradesh 201002, India*

Madhuri T. Patil − *Division of Organic Chemistry, National Chemical Laboratory, Pune 411008, India; PG Department of Chemistry, MCM DAV College for Women, Chandigarh 160036, India*

Nitai Sarkar − *Division of Organic Chemistry, National Chemical Laboratory, Pune 411008, India; Academy of Scientific and Innovative Research, Ghaziabad, Uttar Pradesh 201002, India*

Complete contact information is available at: https://pubs.acs.org/10.1021/acs.cgd.1c00126

Author Contributions

The manuscript was written through the contributions of all authors. All authors have given approval to the final version of the manuscript.

Funding

This work was supported by an Emeritus Scientist grant (21(1090)/19/EMR-II) to MSS from CSIR, New Delhi, India.

Notes

The authors declare no competing financial interest.

ACKNOWLEDGMENTS

NTP and MTP are recipients of fellowships from CSIR, New Delhi; NS is a recipient of fellowships from UGC, New Delhi. This work was supported by an Emeritus Scientist grant (21(1090)/19/EMR-II) to MSS from CSIR, New Delhi, India.

REFERENCES

(1) Brill, Z. G.; Condakes, M. L.; Ting, C. P.; Maimone, T. J. Navigating the Chiral Pool in the Total Synthesis of Complex Terpene Natural Products. *Chem. Rev.* **2017**, *117*, 11753−11795.

(2) Reddy, L. V. R.; Kumar, V.; Sagar, R.; Shaw, A. K. Glycal-Derived δ-Hydroxy α,β-Unsaturated Aldehydes (Perlin Aldehydes): Versatile Building Blocks in Organic Synthesis. *Chem. Rev.* **2013**, *113*, 3605−3631.

(3) Lorenz, H.; Seidel-Morgenstern, A. Processes To Separate Enantiomers. *Angew. Chem., Int. Ed.* **2014**, *53*, 1218−1250.

(4) Nguyen, L. A.; He, H.; Pham-Huy, C. Chiral Drugs: An Overview. *Int. J. Biomed. Sci.* **2006**, *2*, 85−100.

(5) Lo, H. J.; Chang, Y. K.; Yan, T. H. Chiral Pool Based Efficient Synthesis of the Aminocyclitol Core and Furanoside of (−)-Hygromycin A: Formal Total Synthesis of (−)-Hygromycin A. *Org. Lett.* **2012**, *14*, 5896−5899.

(6) Ausmus, A. P.; Hogue, M.; Snyder, J. L.; Rundell, S. R.; Bednarz, K. M.; Banahene, N.; Swarts, B. M. Ferrier Carbocyclization-Mediated Synthesis of Enantiopure Azido Inositol Analogues. *J. Org. Chem.* **2020**, *85*, 3182−3191.

(7) Gannedi, V.; Ali, A.; Singh, P. P.; Vishwakarma, R. A. Total Synthesis of Phospholipomannan of Candida Albicans. *J. Org. Chem.* **2020**, *85*, 7757−7771.

(8) Qiao, L.; Hu, Y.; Nan, F.; Powis, G.; Kozikowski, A. P. A Versatile Approach to PI(3,4)P2, PI(4,5)P2, and PI(3,4,5)P3 from l -(−)-Quebrachitol. *Org. Lett.* **2000**, *2*, 115−117.

(9) Chrzanowska, M.; Grajewska, A.; Rozwadowska, M. D. Asymmetric Synthesis of Isoquinoline Alkaloids 2004−2015. *Chem. Rev.* **2016**, *116*, 12369−12465.

(10) Wu, H.; Wang, W.; Feng, C.; Hou, D. Asymmetric Synthesis of Nabscessin A from Inositol. *J. Org. Chem.* **2020**, *85*, 13153−13159.

(11) Diaz-Muñoz, G.; Miranda, I. L.; Sartori, S. K.; Rezende, D. C.; Diaz, M. A. N. Use of chiral auxiliaries in the asymmetric synthesis of biologically active compounds: A review. *Chirality* **2019**, *31*, 776−812.

(12) Ribeiro, M. F. P.; Pais, K. C.; Jesus, B. S. M.; Fernandez-Lafuente, R.; Freire, D. M. G.; Manoel, E. A.; Simas, A. B. C. Lipase Regioselective O-Acetylations of a *myo*-Inositol Derivative: Efficient Desymmetrization of 1,3-Di-O-Benzyl-myo-Inositol. *Eur. J. Org. Chem.* **2018**, *2018*, 386−391.

(13) Padiyar, L. T.; Zulueta, M. M. L.; Sabbavarapu, N. M.; Hung, S.-C. Yb(OTf) 3 -Catalyzed Desymmetrization of *myo*-Inositol 1,3,5-Orthoformate and Its Application in the Synthesis of Chiral Inositol Phosphates. *J. Org. Chem.* **2017**, *82*, 11418−11430.

(14) Reetz, M. T. Biocatalysis in Organic Chemistry and Biotechnology: Past, Present, and Future. *J. Am. Chem. Soc.* **2013**, *135*, 12480−12496.

(15) Tamura, R.; Iwama, S.; Gonnade, R. G. Control of Polymorphic Transition Inducing Preferential Enrichment. *CrystEngComm* **2011**, *13*, 5269−5280.

(16) Coquerel, G. Preferential Crystallization. *Top. Curr. Chem.* **2006**, *269*, 1−51.

(17) Jacques, J.; Collet, A.; Wilen, S. H. *Enantiomers, Racemates, and Resolutions*; Wiley: New York, 1981; pp 23−31. DOI: 10.1002/bbpc.198200035.

(18) Brandel, C.; Petit, S.; Cartigny, Y.; Coquerel, G. Structural Aspects of Solid Solutions of Enantiomers. *Curr. Pharm. Des.* **2016**, *22*, 4929−4941.

(19) Rekis, T. Crystallization of chiral molecular compounds: what can be learned from the Cambridge Structural Database? *Acta Crystallogr., Sect. B: Struct. Sci., Cryst. Eng. Mater.* **2020**, *B76*, 307−315.

(20) Buhse, T.; Cruz, J.-M.; Noble-Teran, M. E.; Hochberg, D.; Ribo, J. M.; Crusats, J.; Micheau, J.-C. Spontaneous Deracemizations. *Chem. Rev.* **2021**, *121*, 2147−2229.

(21) Clevers, S.; Coquerel, G. Kryptoracemic compound hunting and frequency in the Cambridge Structural Database. *CrystEngComm* **2020**, *22*, 7407−7419.

(22) Zlokazov, M. V.; Pivnitsky, K. K. Lamellar conglomerates. *Mendeleev Commun.* **2020**, *30*, 1−6.

(23) Manna, P.; Jain, S. K. Phosphatidylinositol-3,4,5-Triphosphate and Cellular Signaling: Implications for Obesity and Diabetes. *Cell. Physiol. Biochem.* **2015**, *35*, 1253−1275.

(24) Gillaspy, G. E. The Cellular Language of Myo- Inositol Signaling. *New Phytol.* **2011**, *192*, 823−839.

(25) Corda, D.; Zizza, P.; Varone, A.; Bruzik, K. S.; Mariggiò, S. The Glycerophosphoinositols and Their Cellular Functions. *Biochem. Soc. Trans.* **2012**, *40*, 101−107.

(26) Marat, A. L.; Wallroth, A.; Lo, W. T.; Müller, R.; Norata, G. D.; Falasca, M.; Schultz, C.; Haucke, V. MTORC1 Activity Repression by Late Endosomal Phosphatidylinositol 3,4-Bisphosphate. *Science* **2017**, *356*, 968−972.

(27) Thomas, M. P.; Mills, S. J.; Potter, B. V. L. The "Other" Inositols and Their Phosphates: Synthesis, Biology, and Medicine (with Recent Advances in Myo-Inositol Chemistry). *Angew. Chem., Int. Ed.* **2016**, *55*, 1614−1650.

(28) Shamsuddin, A. M.; Yang, G. Y. *Inositol & Its Phosphates: Basic Science to Practical Applications*; Bentham Science Publishers, 2015.

(29) Conway, S. J.; Miller, G. J. Biology-Enabling Inositol Phosphates, Phosphatidylinositol Phosphates and Derivatives. *Nat. Prod. Rep.* **2007**, *24*, 687−707.

(30) Potter, B. V. L.; Lampe, D. Chemistry of Inositol Lipid Mediated Cellular Signaling. *Angew. Chem., Int. Ed. Engl.* **1995**, *34*, 1933−1972.

(31) Sureshan, K. M.; Shashidhar, M. S.; Praveen, T.; Das, T. Regioselective Protection and Deprotection of Inositol Hydroxyl Groups. *Chem. Rev.* **2003**, *103*, 4477−4504.

(32) Watanabe, Y. Synthetic Strategies Based on Phosphite Chemistry Aiming at Efficient Synthesis of Inositol Phospholipids. *Yuki Gosei Kagaku Kyokaishi* **2000**, *58*, 1057−1065.

(33) Parthasarathy, R.; Eisenberg, F. Biochemistry, Stereochemistry, and Nomenclature of the Inositol Phosphates. *ACS Symp. Ser.* **1991**, *463*, 1−19.

(34) Gurale, B. P.; Sardessai, R. S.; Shashidhar, M. S. Myo-Inositol 1,3-Acetals as Early Intermediates during the Synthesis of Cyclitol Derivatives. *Carbohydr. Res.* **2014**, *399*, 8−14.

(35) Olsson, S.; Björemark, P. M.; Kokoli, T.; Sundberg, J.; Lennartson, A.; McKenzie, C. J.; Håkansson, M. Absolute Asymmetric Synthesis: Protected Substrate Oxidation. *Chem. - Eur. J.* **2015**, *21*, 5211−5219.

(36) Praveen, T.; Puranik, V. G.; Shashidhar, M. S. Synthesis and Structure of (±)-4-O-Methanesulfonyl-Myo-Inositol 1,3,5-Orthoformate. *J. Chem. Crystallogr.* **2000**, *30*, 605−609.

(37) Moon, S. C.; Echeverría, G. A.; Punte, G.; Ellena, J.; Bruno-Blanch, L. E. Crystal Structure and Anticonvulsant Activity of (±)-1,2:4,5-Di-O-Isopropylidene-3,6-Di-O-(2-Propylpentanoyl)-Myo-Inositol. *Carbohydr. Res.* **2007**, *342*, 1456−1461.

(38) Krishnaswamy, S.; Gonnade, R. G.; Bhadbhade, M. M.; Shashidhar, M. S. Two Modes of O—H···O Hydrogen Bonding Utilized in Dimorphs of Racemic 6- O -Acryloyl-2- O -Benzoyl- Myo -Inositol 1,3,5-Orthoformate. *Acta Crystallogr., Sect. C: Cryst. Struct. Commun.* **2009**, *C65*, o54−o57.

(39) Jagdhane, R. C. Synthesis of Cyclitols and Their Analogs from Naturally Occurring Inositols. Ph. D. Thesis, University of Pune, 2010.

(40) Gainsford, G. J.; Lensink, C.; Falshaw, A.; Mee, S. P. H. 1-Amino-1-Deoxy-2,3,4,5-Tetra-O-Methyl Scyllo-Inositol. *Acta Crystallogr., Sect. E: Struct. Rep. Online* **2006**, *E62*, o5411−o5413.

(41) Sureshan, K. M.; Murakami, T.; Miyasou, T.; Watanabe, Y. Topochemical Transketalization Reaction Driven by Hydrogen Bonding. *J. Am. Chem. Soc.* **2004**, *126*, 9174−9175.

(42) Devaraj, S.; Shashidhar, M. S.; Dixit, S. S. Chelation Controlled Regiospecific O-Substitution of Myo-Inositol Orthoesters: Convenient Access to Orthogonally Protected Myo-Inositol Derivatives. *Tetrahedron* **2005**, *61*, 529−536.

(43) Fabian, L.; Brock, C. P. A List of Organic Kryptoracemates. *Acta Crystallogr., Sect. B: Struct. Sci.* **2010**, *B66*, 94−103.

https://doi.org/10.1021/acs.cgd.1c00126
Cryst. Growth Des. 2021, 21, 3786−3797

(44) Sureshan, K. M.; Shashidhar, M. S.; Praveen, T.; Gonnade, R. G.; Bhadbhade, M. Regioselective Sulfonylation of Myo -Inositol Orthoesters. *Carbohydr. Res.* **2002**, *337*, 2399−2410.
(45) Sureshan, K. M.; Das, T.; Shashidhar, M. S.; Gonnade, R. G.; Bhadbhade, M. M. Sulfonate Protecting Groups: Synthesis of D- and L-*Myo*-Inositol-1,3,4,5-Tetrakisphosphate Precursors. *Eur. J. Org. Chem.* **2003**, *2003*, 1035−1041.
(46) Sarmah, M. P.; Shashidhar, M. S.; Sureshan, K. M.; Gonnade, R. G.; Bhadbhade, M. M. Synthesis of O- and C-Methylated Inositols: D- and L-Ononitol, D- and L-Laminitol, Mytilitol and Scyllo-Inositol Methyl Ether. *Tetrahedron* **2005**, *61*, 4437−4446.
(47) Sureshan, K. M; Shashidhar, M. S Sulfonate Protecting Groups. Regioselective *O*-Sulfonylation of Myo-Inositol Orthoesters. *Tetrahedron Lett.* **2001**, *42*, 3037−3039.
(48) Patil, N. T.; Shashidhar, M. S.; Gonnade, R. G.; Patil, M. T. Rapid Access to Chiral Inositol Derivatives Having Orthogonal Functional Groups via the Resolution of a Racemic Myo-Inositol Orthoformate Derivative without the Aid of Chiral Resolving Agents. Indian Patent application 201711010407, 2018.
(49) Laumen, K.; Ghisalba, O. Chemo-Enzymatic Synthesis of Both Enantiomers of Myo -Inositol 1,3,4,5-Tetrakisphosphate. *Biosci., Biotechnol., Biochem.* **1999**, *63*, 1374−1377.
(50) Mislow, K. Absolute Asymmetric Synthesis: A Commentary. *Collect. Czech. Chem. Commun.* **2003**, *68*, 849−864.
(51) Weissbuch, I.; Lahav, M. Crystalline Architectures as Templates of Relevance to the Origins of Homochirality. *Chem. Rev.* **2011**, *111*, 3236−3267.
(52) Gavezzotti, A. Are Crystal Structures Predictable? *Acc. Chem. Res.* **1994**, *27*, 309−314.
(53) Gavezzotti, A.; Filippini, G. Geometry of the Intermolecular X-H···Y (X, Y = N, O) Hydrogen Bond and the Calibration of Empirical Hydrogen-Bond Potentials. *J. Phys. Chem.* **1994**, *98*, 4831−4837.
(54) Macrae, C. F.; Sovago, I.; Cottrell, S. J.; Galek, P. T. A.; McCabe, P.; Pidcock, E.; Platings, M.; Shields, G. P.; Stevens, J. S.; Towler, M.; Wood, P. A. Mercury 4.0: from visualization to analysis, design and prediction. *J. Appl. Crystallogr.* **2020**, *53*, 226−235.
(55) Donnay, J. D. H.; Harker, D. A new law of crystal morphology extending the law of Bravais. *Am. Mineral.* **1937**, *22*, 446−467.
(56) Prywer, J. Explanation of some peculiarities of crystal morphology deduced from the BFDH law. *J. Cryst. Growth* **2004**, *270*, 699−710.
(57) Patil, N. T.; Shashidhar, M. S.; Tamboli, M. I.; Gonnade, R. G. Clues from Crystal Structures Pave the Way to Access Chiral Myo -Inositol Derived Versatile Synthons: Resolution of Racemic 4- O -Allyl- Myo -Inositol-1,3,5-Orthoesters via Corresponding Dicamphanates by Crystallization. *Cryst. Growth Des.* **2017**, *17*, 5432−5440.
(58) Weissbuch, I.; Lahav, M.; Leisorowitz, L. Tailor-Made" And Charge-Transfer Auxiliaries for the Control of The Crystal Polymorphism of Glycine. *Adv. Mater.* **1994**, *6*, 952−956.
(59) Davey, R. J.; Blagden, N.; Potts, G. D.; Docherty, R. Polymorphism in Molecular Crystals: Stabilization of a Metastable Form by Conformational Mimicry. *J. Am. Chem. Soc.* **1997**, *119*, 1767−1772.
(60) Wallach, O. Zur Kenntniss der Terpene und der ätherischen Oele. *Liebigs Ann. Chem.* **1895**, *286*, 90−143.
(61) Brock, C. P.; Schweizer, W. B.; Dunitz, J. D. On the Validity of Wallach's Rule: On the Density and Stability of Racemic Crystals Compared with Their Chiral Counterparts. *J. Am. Chem. Soc.* **1991**, *113*, 9811−9820.
(62) Parsons, S. Introduction to Twinning. *Acta Crystallogr., Sect. D: Biol. Crystallogr.* **2003**, *59*, 1995−2003.
(63) Flack, H. D. Louis Pasteur's Discovery of Molecular Chirality and Spontaneous Resolution. *Acta Crystallogr., Sect. A: Found. Crystallogr.* **2009**, *A65*, 371−389.
(64) Sogutoglu, L.-C.; Steendam, R. R. E.; Meekes, H.; Vlieg, E.; Rutjes, F. P. J. T. Viedma Ripening: a Reliable Crystallisation Method to Reach Single Chirality. *Chem. Soc. Rev.* **2015**, *44*, 6723−6732.
(65) Perez-Garcia, L.; Amabilino, D. B. Spontaneous resolution, whence and whither: from enantiomorphic solids to chiral liquid crystals, monolayers and macro- and supra-molecular polymers and assemblies. *Chem. Soc. Rev.* **2007**, *36*, 941−967.
(66) Coquerel, G.; Hoquante, M. Spontaneous and Controlled Macroscopic Chiral Symmetry Breaking by Means of Crystallization. *Symmetry* **2020**, *12*, 1796−1818.
(67) Bredikhin, A. A.; Bredikhina, Z. A. Stereoselctive crystallization as a basis for single enantiomer drug production. *Chem. Eng. Technol.* **2017**, *40*, 1211−1220.
(68) Lorenz, H.; Polenske, D.; Seidel-Morgenstern, A. Application of Preferential Crystallization to Resolve Racemic Compounds in a Hybrid Process. *Chirality* **2006**, *18*, 828−840.
(69) Kaji, Y.; Uemura, N.; Kasashima, Y.; Ishikawa, H.; Yoshida, Y.; Mino, T.; Sakamoto, M. Asymmetric Synthesis of an Amino Acid Derivative from Achiral Aroyl Acrylamide by Reversible Michael Addition and Preferential Crystallization. *Chem. - Eur. J.* **2016**, *22*, 16429−16432.
(70) Johansson, A.; Håkansson, M. Absolute Asymmetric Synthesis of Stereochemically Labile Aldehyde Helicates and Subsequent Chirality Transfer Reactions. *Chem. - Eur. J.* **2005**, *11*, 5238−5248.
(71) Sakamoto, M. Absolute Asymmetric Synthesis from Achiral Molecules in the Chiral Crystalline Environment. *Chem. - Eur. J.* **1997**, *3*, 685−689.

https://doi.org/10.1021/acs.cgd.1c00126
Cryst. Growth Des. 2021, 21, 3786−3797